Supporting Information for

The First Chiral Cerium Halide towards Circularly-polarized Luminescence in the UV Region

Xinyi Niu,# Zhichao Zeng,# Zhaoyu Wang, Haolin Lu, Bing Sun, Hao-Li Zhang, Yongsheng Chen, Yaping Du* and Guankui Long*

Experimental Section

Chemicals:

The chemicals including $CeCl_3$ (99.99%, Heowns), (*R*/*S*)-(+)-α-methylbenzylamine (99%, Adamas), hydrochloric acid (37%, Aladdin), diethyl ether (99.8%, Tianjin Bohua Chemical Reagent), and ultra-dry methanol (water <30 ppm) (99.9%, J&K Scientific) were used as received without any further purification.

Growth of *R*/*S*-MCC single crystals:

$CeCl_3$ (99.99%), *R*/*S*-α-methylbenzylamine, and hydrochloric acid were mixed at molar ratios of 1/1/1.2 in a flask with 1 mL of anhydrous methanol. The mixture was heated to 50 °C and stirred for 1 hour. Then, the temperature was increased to fully remove the solvent and obtain a solid precursor. Afterward, the precursor was dissolved in anhydrous methanol and crystallized using diethyl ether as the antisolvent to obtain *R*/*S*-MCC single crystals.

Characterization:

Powder X-ray diffraction (PXRD) patterns of *R*/*S*-MCC were obtained on a Rigaku Smart Lab 3 kW (Cu Kα) diffractometer. The single-crystal X-ray diffraction data were collected at 100 K on a Rigaku XtaLAB PRO MM007 DW single-crystal X-ray diffractometer (Cu-Kα, λ=1.54178 Å). The crystal structures were solved using Olex2 software.[1] The X-ray crystallographic structures have been deposited at the Cambridge Crystallographic Data Centre (CCDC No. 2327202 and No. 2327203 for *R*-MCC and *S*-MCC), and can be obtained free of charge from the CCDC via www.ccdc.cam.ac.uk/ get structures.

X-ray photoelectron spectroscopy (XPS) data were obtained on a Thermo Scientific ESCALAB 250Xi (Al Kα) spectrometer. A scanning electron microscope (SEM) (JEOL JSM-7800F) with an attached energy dispersive spectrometer was used to observe the morphology and elemental distribution of the samples.

The absorption spectra of the samples were collected on a Shimadzu UV-2600 UV-Vis spectrometer. An Edinburgh FLS 1000 spectrometer (with a 450 W xenon lamp, nanosecond flash lamp, and an integrating sphere) was used to measure the photoluminescence (PL) excitation-emission maps and emission spectra, PL decay curves of *R*/*S*-MCC. We employed the UV lamp (303 nm) as the excitation light source for the PL measurements (detective range from 330 to 500 nm). The PL lifetime of the samples was measured with a nanosecond flash lamp at 312 nm. The PL quantum yield (QY) was measured by Edinburgh FLS 1000 spectrometer with an integrating sphere, via the absolute method (λ_{ex} = 303 nm, integrating the emission spectra from 340 to 420 nm). Circular dichroism (CD) and linear dichroism (LD) spectra were obtained on a JASCO J-1500 CD spectrometer. KBr powder and *R*/*S*-MCC powder were used and pressed into pellets for CD analysis. The VCD spectrum was measured on BRUKER PMA50, INVENIO-R vibration circular dichroic-infrared spectrometer by using a mixture of KBr and *R/S*-MCC pellets. Magnetic susceptibility curves of the samples were recorded on a Quantum Design MPMS3 SQUID magnetometer. Fourier transform infrared (FT-IR) spectra of the samples were obtained on a Brucker-Tensor 37 IR spectrometer by using a mixture of KBr and *R/S*-MCC pellets. Circularly polarized photoluminescence (CPL) measurements were conducted on a JASCO CPL-300 spectrometer by using a mixture of KBr and *R/S*-MCC pellets.

The Vienna *ab initio* simulation package (VASP) software under the framework of density functional theory (DFT)[2, 3] was used to perform the calculations. The projector augmented-wave (PAW)[4] method is used to process the electrons near the nucleus, and the Perdew-Burke-Ernzerh (PBE) functional, as revised for solids (PBEsol)[5], is selected. The plane-wave cut-off energy was set to 500 eV. All the structures were fully relaxed until the energy and total forces converged to 10^{-5} eV and 0.001 eV/Å, respectively. The DFT-D3 method with Becke-Johnson damping (BJ)[6] was applied for van der Waals correction. The initial magnetic moments of a net spin electron in each of the Ce^{3+} are set to be opposite for spin polarization calculations. Γ-centred Monkhorst-Pack mesh k points with k-spacing of 0.04π $Å^{-1}$ is employed for sampling the Brillouin zones for the calculations of the static, absorption, and projected density of states (DOS) of elements. For the electronic band structures calculations, 20 inserted K-points between each pair of high symmetry points were used. The VASPKIT code[7] was used for post-processing analysis.

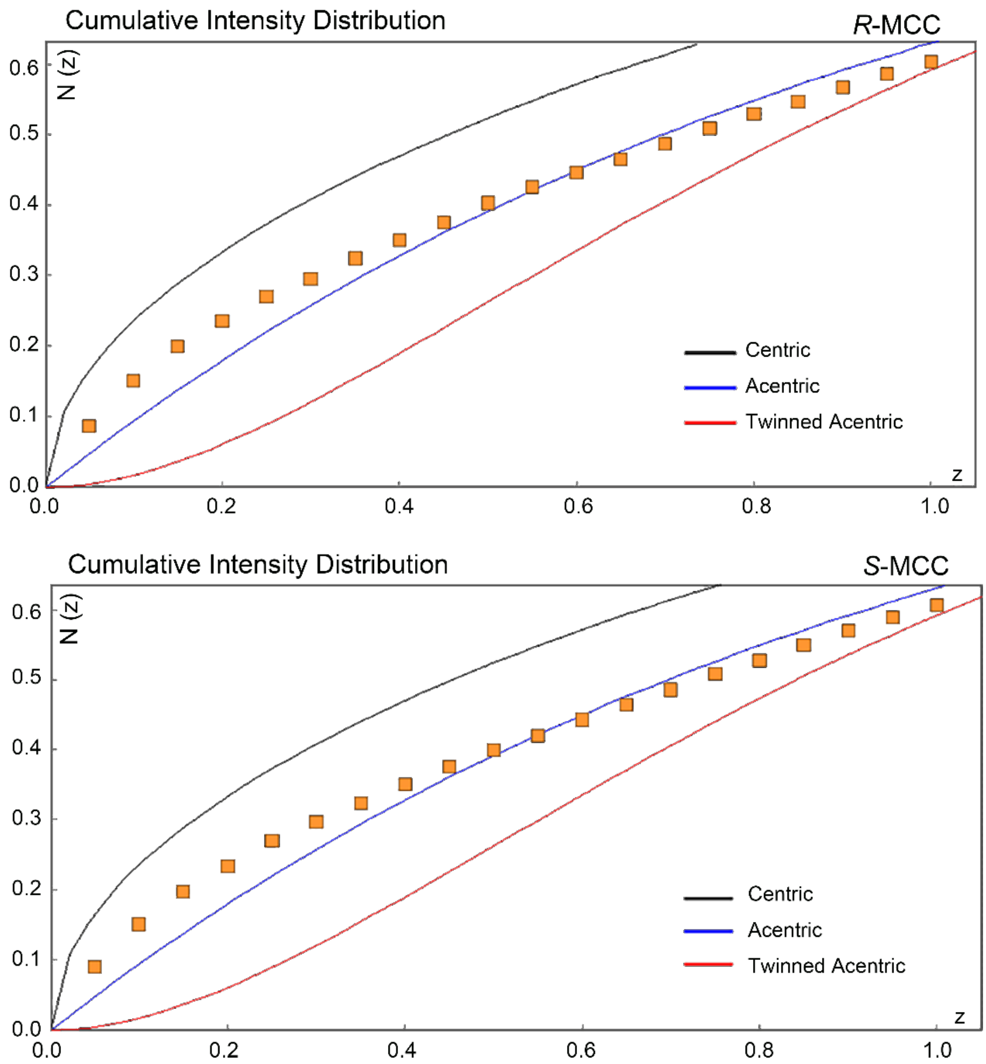

Figure S1. The cumulative intensity distribution of the single crystal X-ray diffraction data for *R*-/*S*-MCC. Note that the inorganic framework scatters X-rays more strongly than does the organic framework, and the cumulative intensity distribution therefore preferentially reflects the symmetry of the inorganic framework.

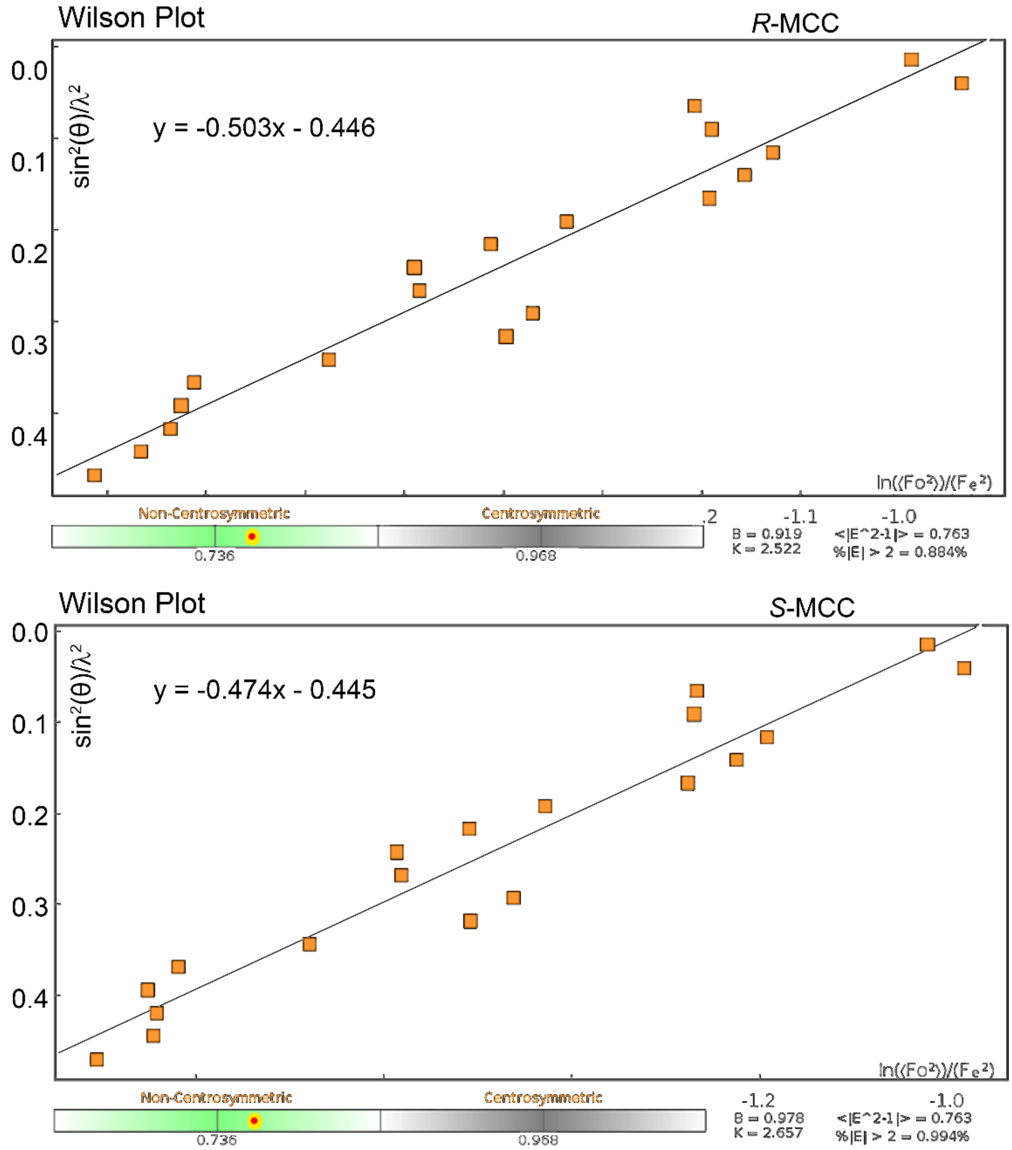

Figure S2. Wilson statistics obtained during reduction of single-crystal X-ray diffraction data for *R*-/*S*-MCC. The statistics give <$|E^2$-1|> values of 0.763 for the *R*-MCC and 0.763 for the *S*-MCC. Note that the inorganic framework scatters X-rays more strongly than the organic framework, and the Wilson statistics therefore preferentially reflect the symmetry of the inorganic framework.

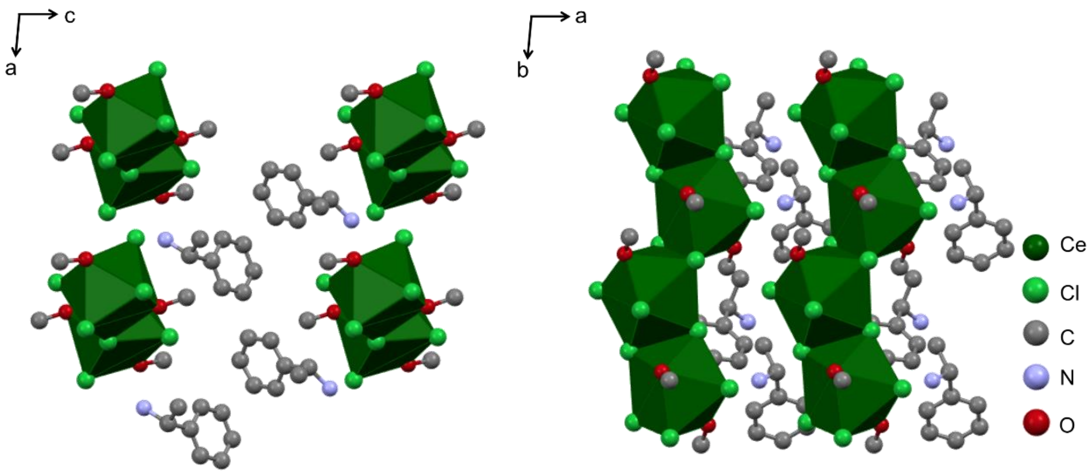

Figure S3. The packing structure of *R*-MCC viewed along the *b*- and *c*-axes.

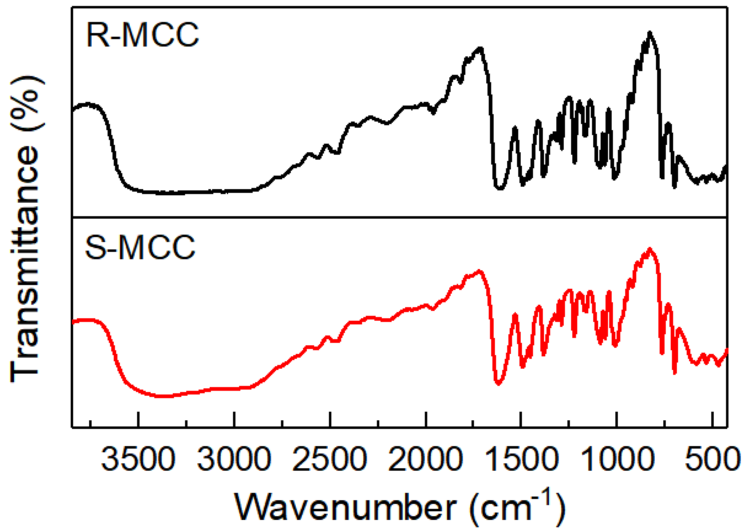

Figure S4. The FT-IR spectra of *R*/*S*-MCC.

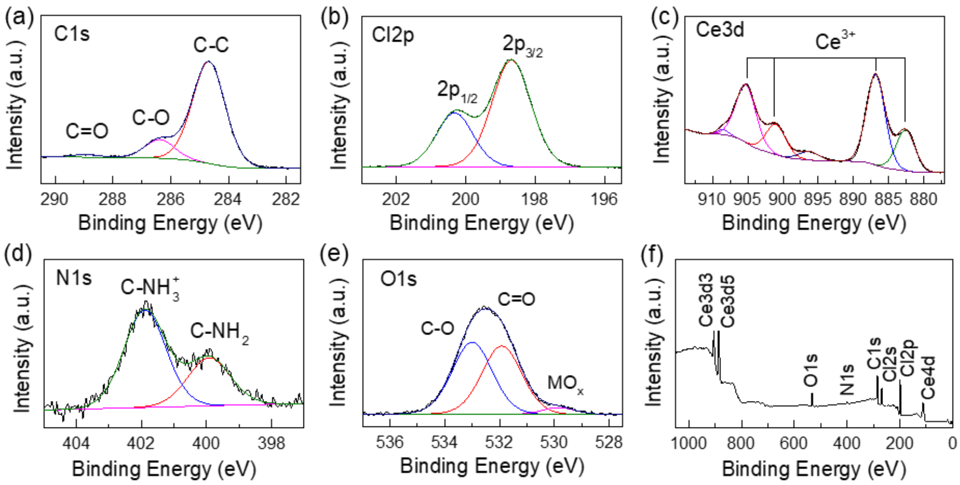

Figure S5. The High-resolution XPS spectra of (a) C 1*s*, (b) Cl 2*p*, (c) Ce 3*d*, (d) N 1*s* and (e) O 1*s* in *R*-MCC. (f) XPS spectrum of *R*-MCC.

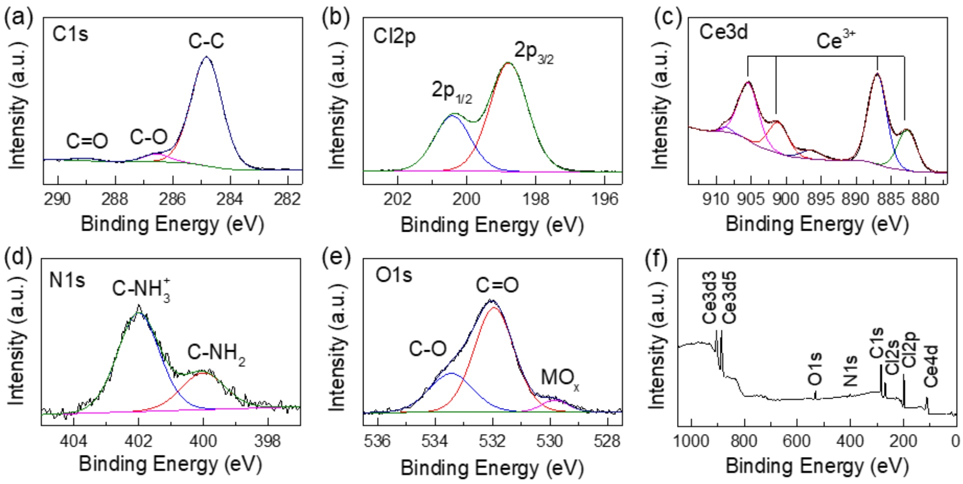

Figure S6. (a-e) The High-resolution XPS spectra of (a) C 1*s*, (b) Cl 2*p*, (c) Ce 3*d*, (d) N 1*s* and (e) O 1*s* in *S*-MCC. (f) XPS spectrum of *S*-MCC.

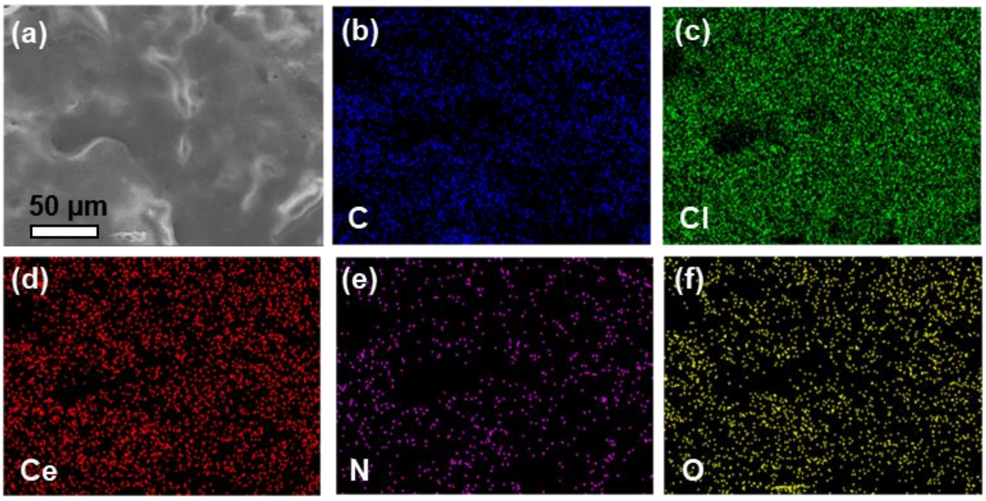

Figure S7. SEM image of the (a) crushed *R*-MCC crystal, (b-f) EDS mapping of C, Cl, Ce, N and O.

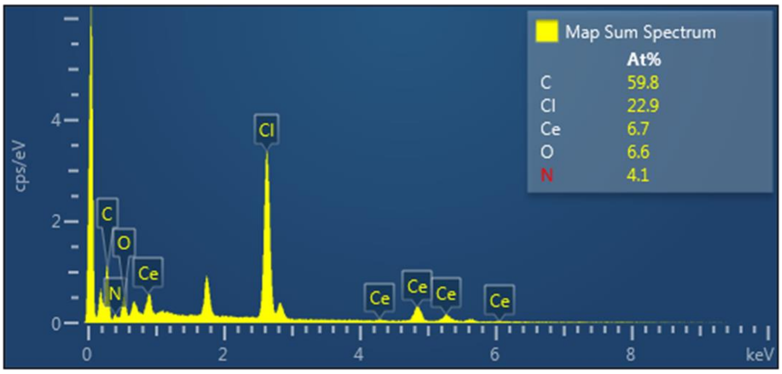

Figure S8. The EDS spectrum of *R*-MCC.

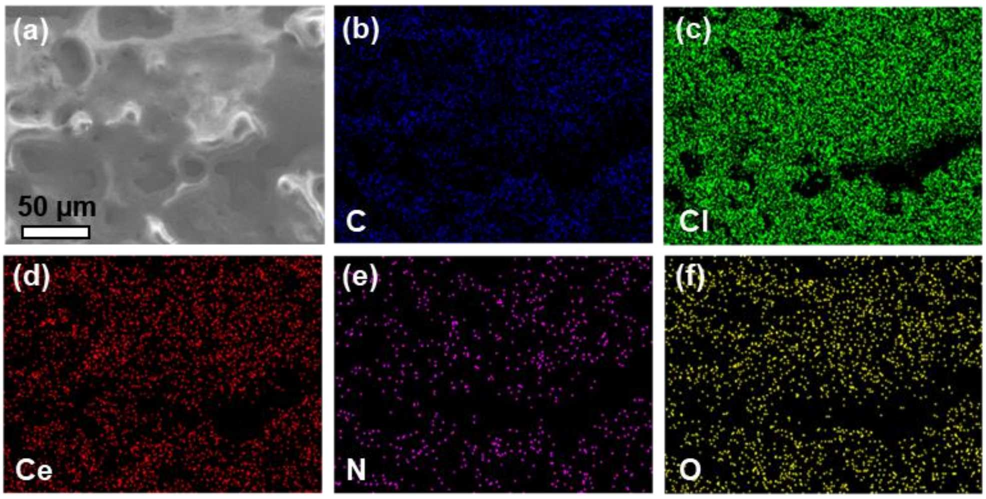

Figure S9. SEM image of the (a) crushed *S*-MCC crystal, (b-f) EDS mapping of C, Cl, Ce, N and O.

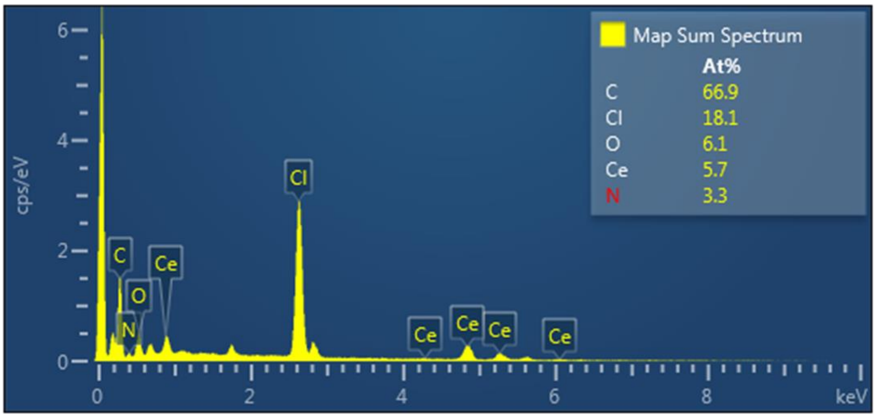

Figure S10. The EDS spectrum of *S*-MCC.

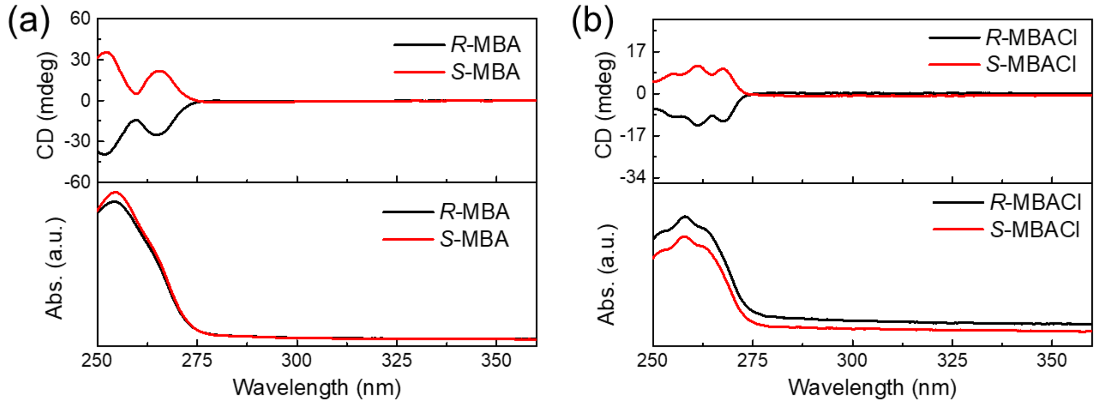

Figure S11. The CD and absorption spectra of (a) *R/S*-MBA and (b) *R/S*-MBACl.

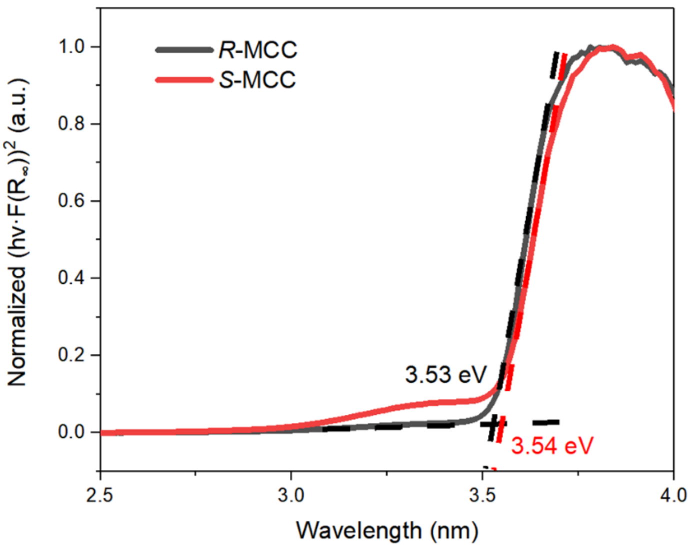

Figure S12. The calculated band gap of *R*/*S*-MCC by the *Tauc* plot.

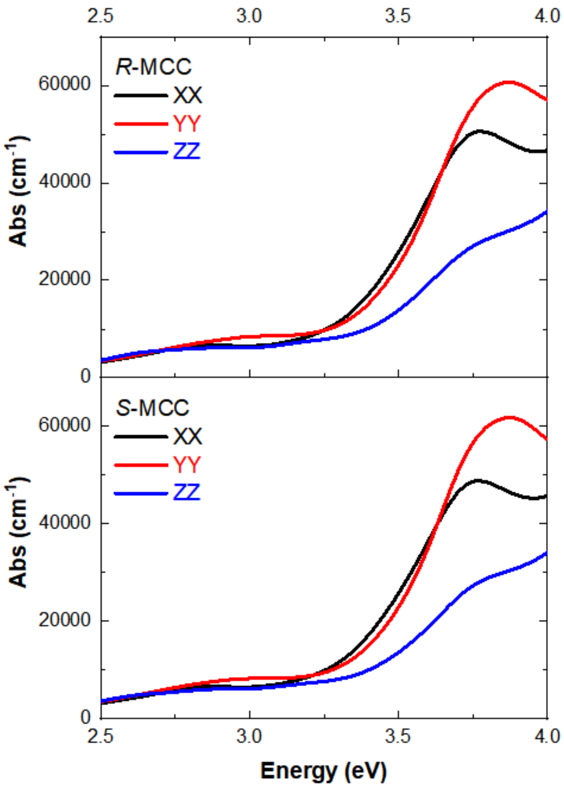

Figure S13. The calculated absorption spectra of *R/S*-MCC.

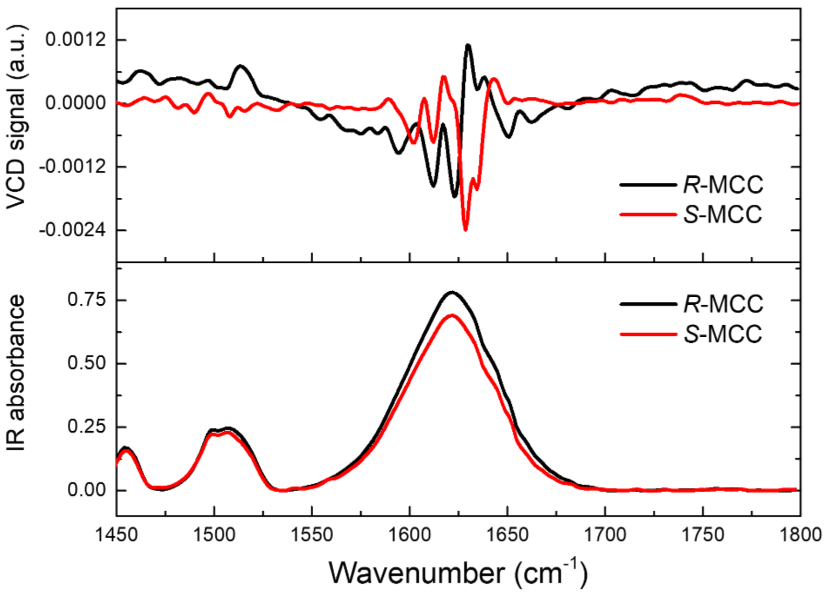

Figure S14. The VCD and FT-IR spectra of *R*-MCC and *S*-MCC.

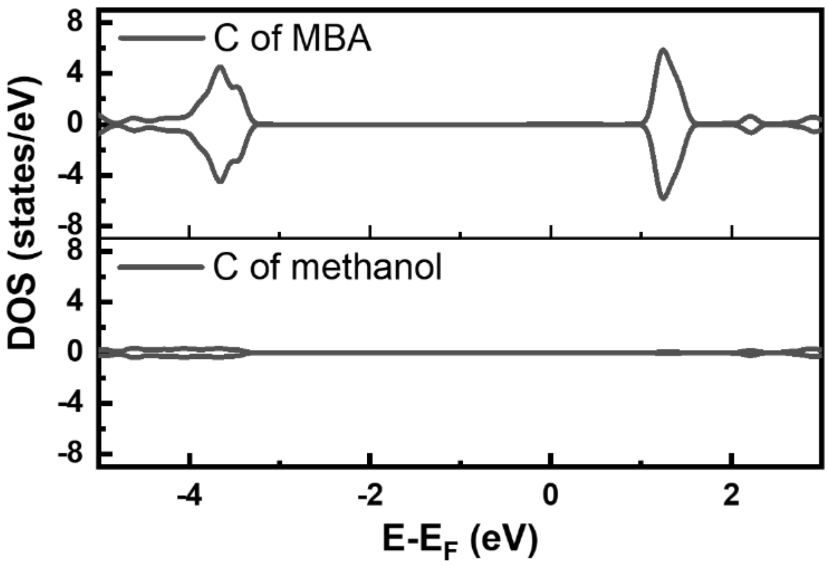

Figure S15. The PDOS diagrams of C element in methanol and MBA in *R*-MCC.

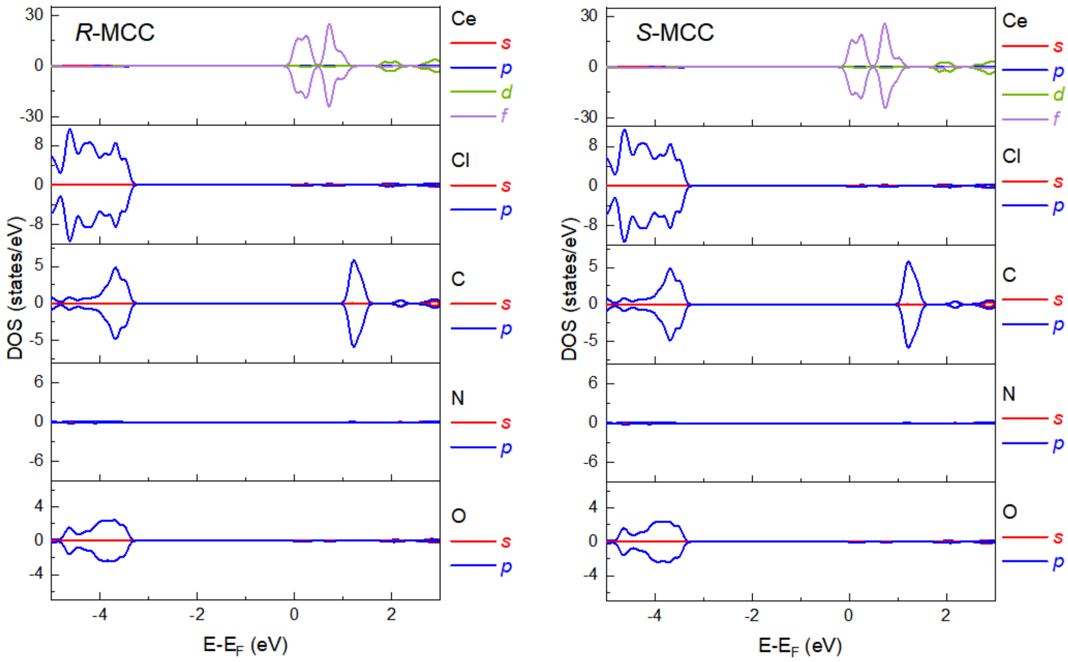

Figure S16. The PDOS diagrams of all elements in *R/S*-MCC.

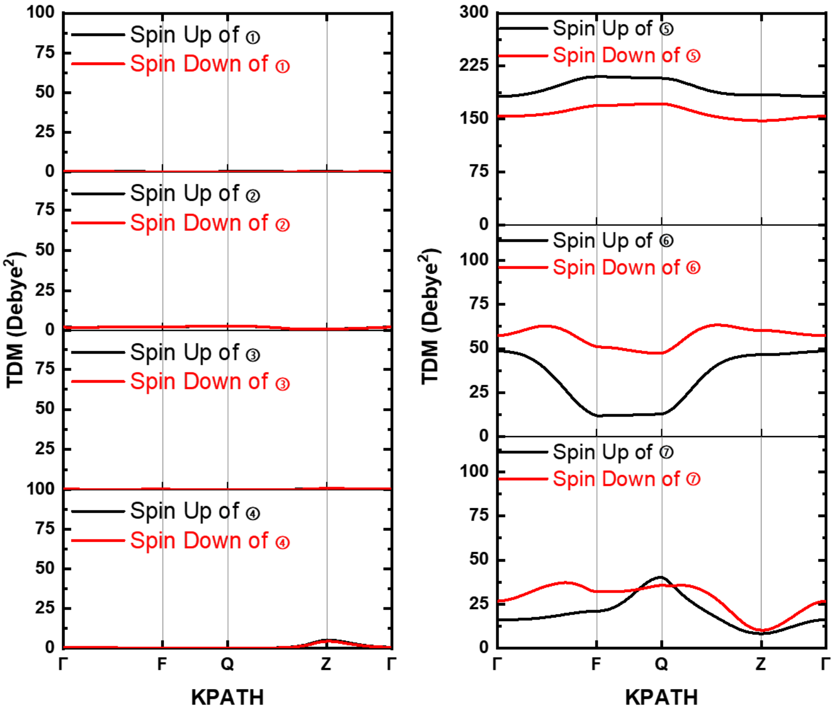

Figure S17. The diagram of TDMs of *R*-MCC.

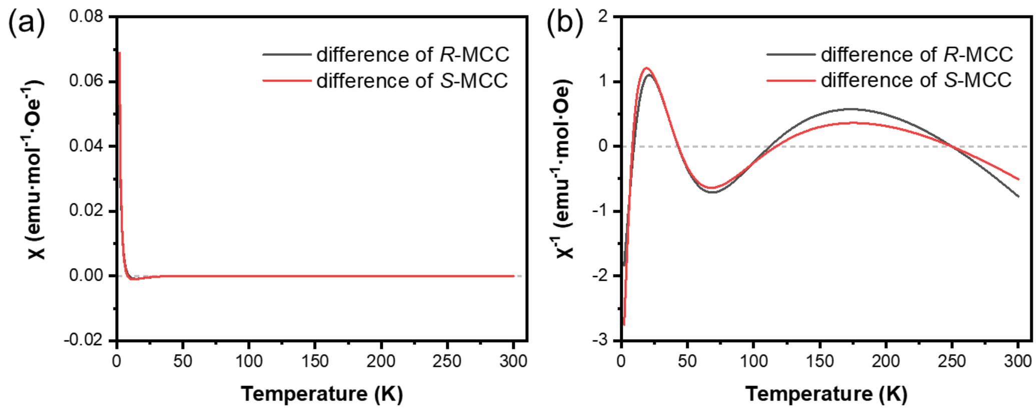

Figure S18. The difference between the 3-level equation and the 2-level equation of the susceptibility (a) and the inverse susceptibility (b).

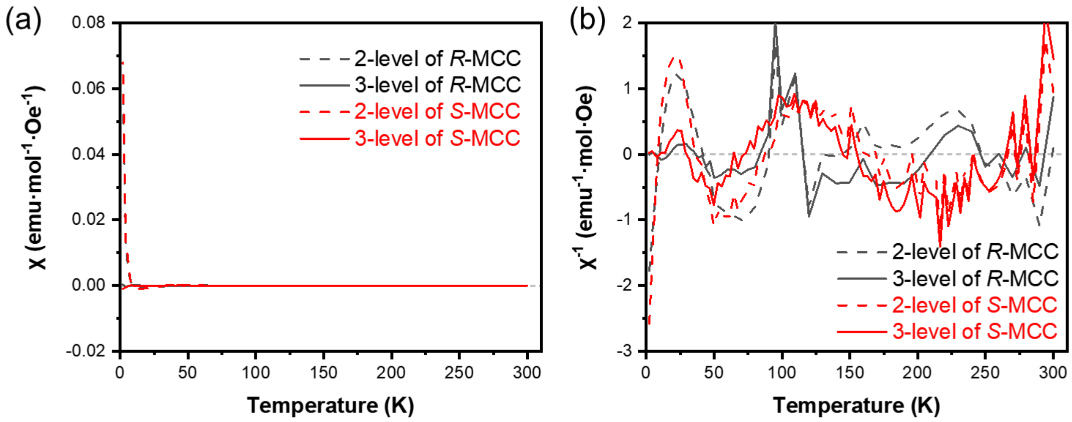

Figure S19. The difference between the experimental data and the 2-/3-level equation of the susceptibility (a) and the inverse susceptibility (b).

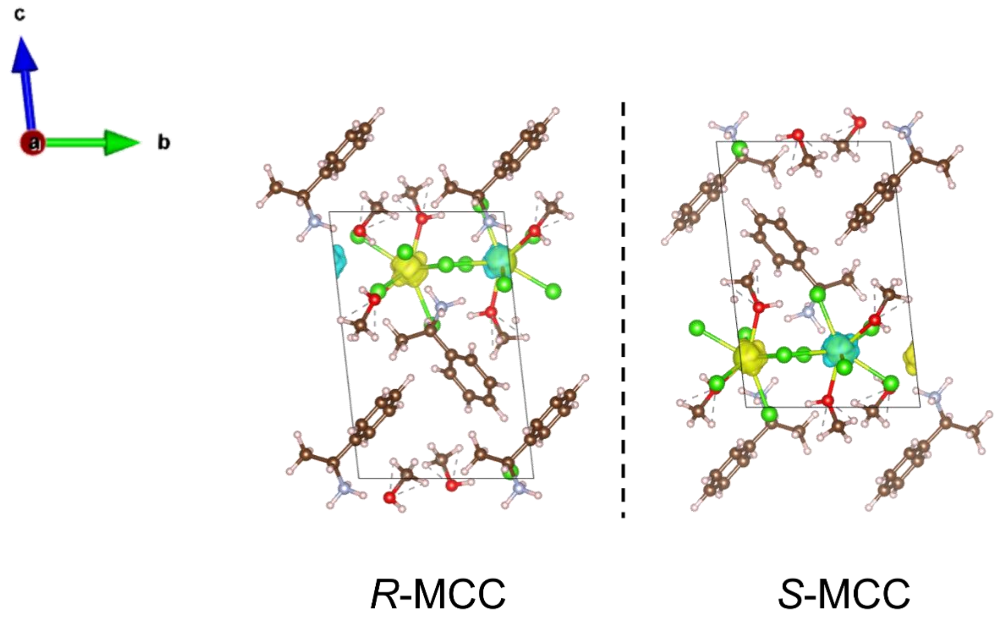

Figure S20. The calculated spin densities of *R/S*-MCC.

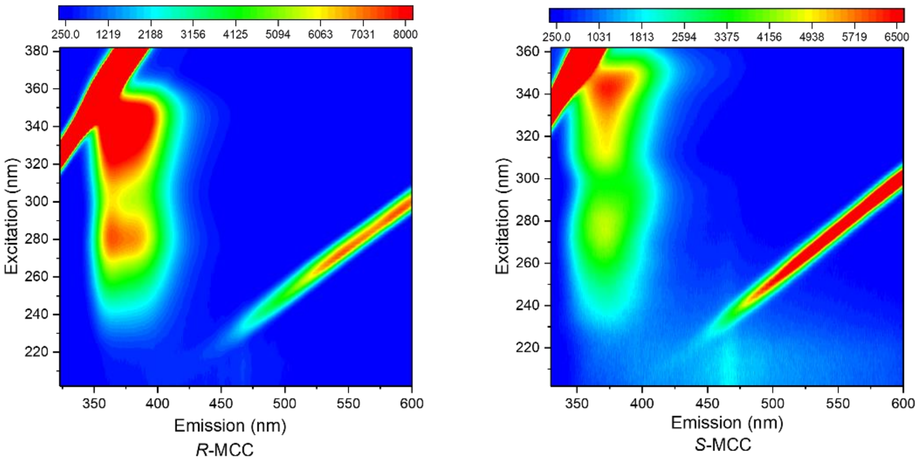

Figure S21. The PL excitation-emission maps of *R*/*S*-MCC.

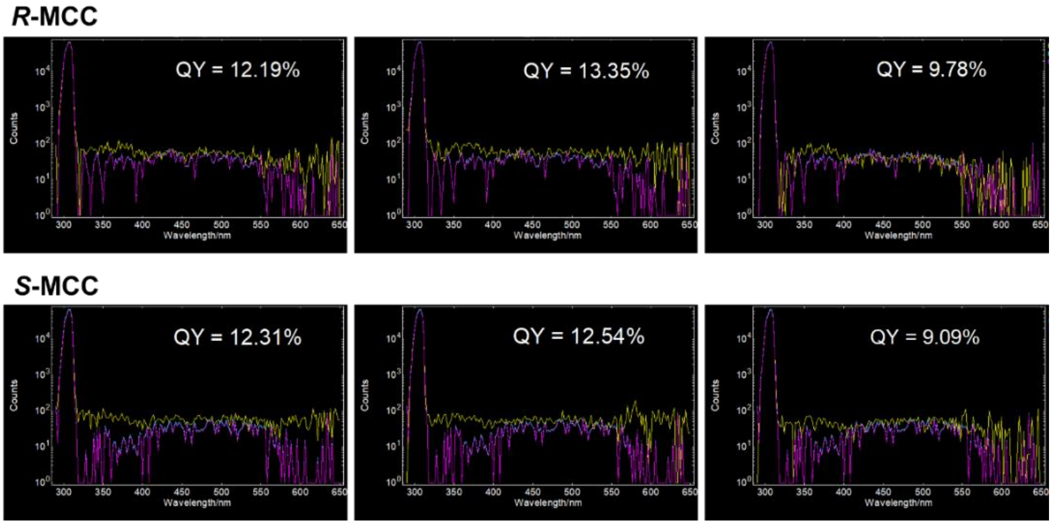

Figure S22. The PLQY of *R/S*-MCC.

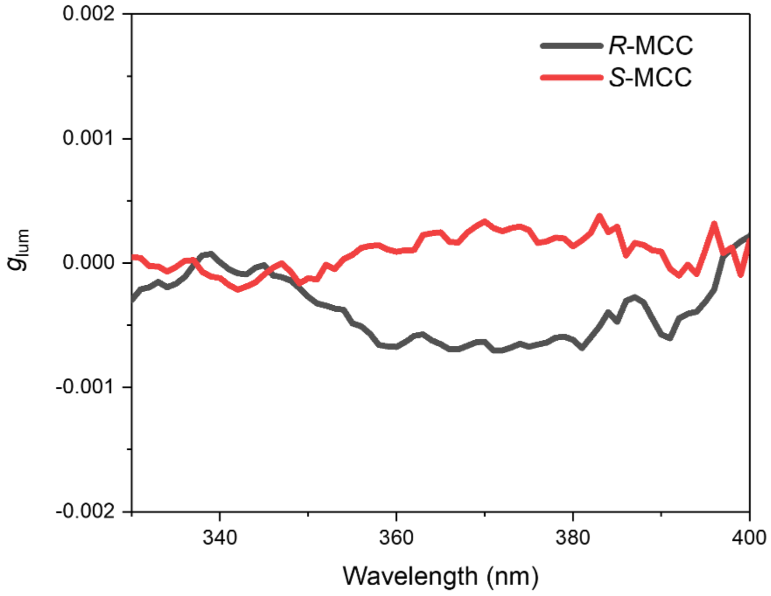

Figure S23. The g_{lum} spectra of *R/S*-MCC.

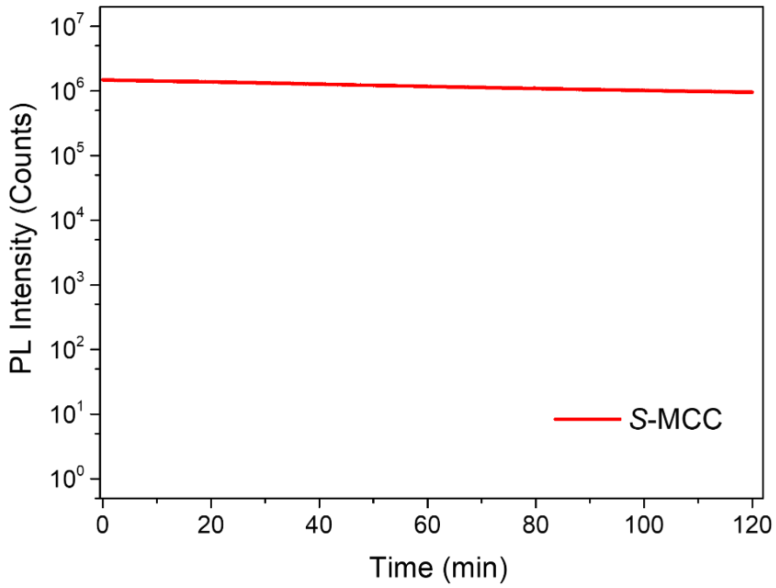

Figure S24. The luminescence intensity at 364 nm of *S*-MCC under constant UV irradiation at 348nm.

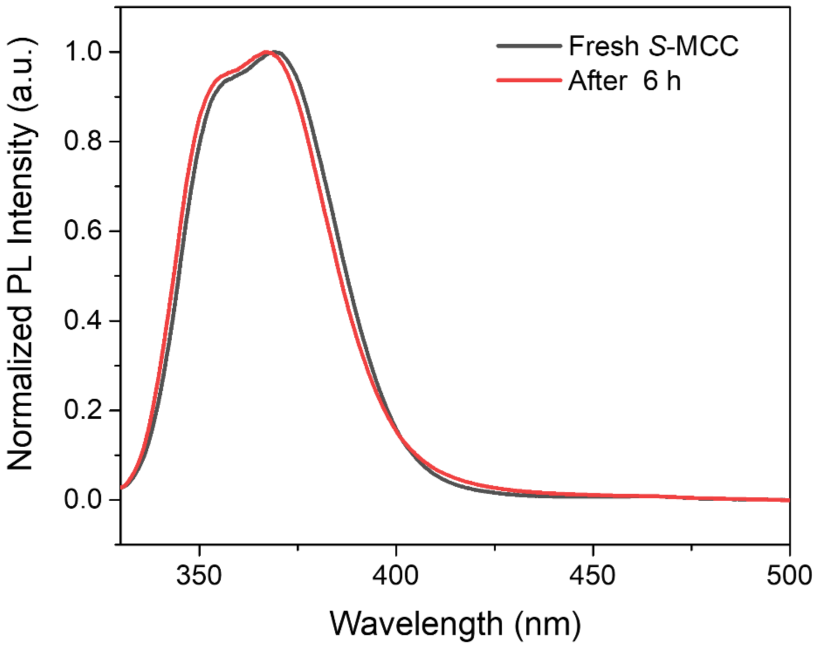

Figure S25. The PL spectra of *S*-MCC before and after heating at 60 °C for 6 hours.

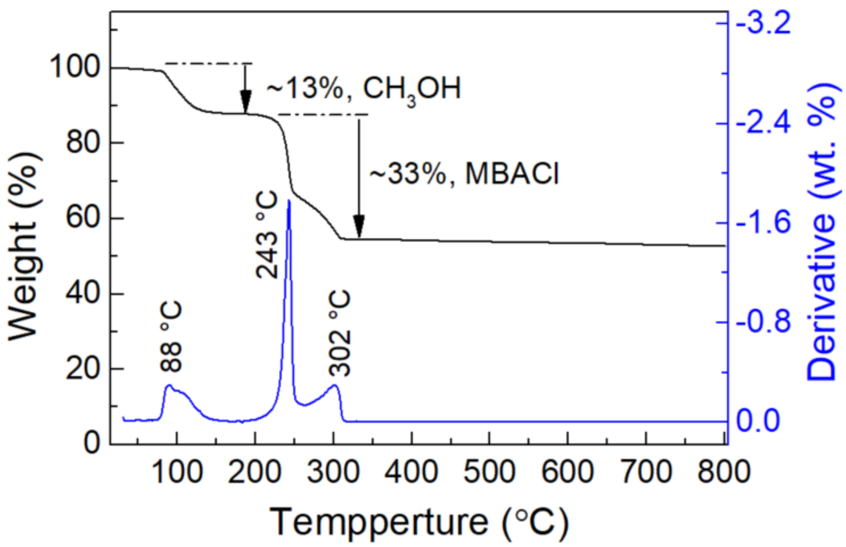

Figure S26. TGA curve of *S*-MCC.

Table S1. The parameters of some representative CPL materials in OIHMHs.

	CPL Materials	λ_{em} (nm)	g_{lum}	PLQY	Ref.
1	(R/S-$C_6H_{16}N_2$)$PbBr_4$	550	±0.2%	1.33/1.44%	[8]
2	(R/S-MBA)$_4Cu_4I_8\cdot 2H_2O$ SC	519	±0.15%	21.44%/21.84%	[9]
3	(R/S-3-fluoropyrrolidinium)$_3MnBr_3$	650	±0.61%	28.13%/32.46%	[10]
4	(R/S- 3AP)$PbBr_3Cl\cdot H_2O$	575	4%/−3.6%	27.6%/25.7%	[11]
5	[R/S-(H_2MPz)]$_3Pb_2Br_{10}\cdot$2DMAc	550	±0.3%	16.38%/14.18%	[12]
6	(R/S-1-PPA)$_2MnBr_4$	510	−1%/0.8%	9.35%/13.24%	[13]
7	(R/S-3-quinuclidinol)$MnBr_3$ Polycrystalline	625	2.3%/−2.27%	31.6%,	[14]
8	(R/S-MBA)$_4Cu_4I_4$	630	1%/−0.6%	60%	[15]
9	(R/S-BPEA)FA$PbBr_4\cdot H_2O$	430	±0.84%	7.9%	[16]
10	(R/S-MBA)$MnCl_3\cdot CH_3OH$	660	±1.25%	/	[17]
11	$DMA_4[InCl_6]Br$	585	±0.5%	81.4%	[18]
12	(R-CHEA)$_4In_{1.35}Sb_{0.65}Cl_{10}$	710	−1.53%	6.8%	[19]
13	(R/S-FMBA)$_2PbBr_4$ Powder	525	0.19%	5.19%/6.21%	[20]
14	R/S-PbSnBr$\cdot H_2O$ SC	580	±0.3%	100%	[21]
	R/S-MCC	370	−0.0633% /0.0334%	11.7±1.0%/11.3 ±1.1%	**This work**

Table S2. Crystal data and structural refinement of *R*/*S*-MCC.

Compounds	*R*-MCC	*S*-MCC
Formula	$C_{10}H_{20}CeCl_4NO_2$	$C_{10}H_{20}CeCl_4NO_2$
Temperature (*K*)	100.00(10)	100.00(10)
Crystal system	triclinic	triclinic
Space group	*P*1	*P*1
a (Å)	8.22330(10)	8.2204(2)
b (Å)	8.52450(10)	8.51930(10)
c (Å)	12.9148(2)	12.9253(2)
α (°)	94.7450(10)	94.7900(10)
β (°)	96.5800(10)	96.7290(10)
γ (°)	97.6220(10)	97.616(2)
Volume (Å^3)	886.99(2)	886.50(3)
Z	2	2
ρ_{calc} g/cm^3	1.753	1.754
μ/mm^{-1}	3.162	3.164
F(000)	458.0	458.0

Table S3. Bond Lengths for *R*-MCC.

Atom	Atom	Length/Å	Atom	Atom	Length/Å
Ce01	Cl03	2.8472(14)	C00N	C00Z	1.377(7)
Ce01	Cl04	2.8634(15)	C00Q	C00S	1.529(7)
Ce01	Cl05	2.9131(15)	C00Q	C00X	1.508(7)
Ce01	Cl06	2.7975(14)	C00Q	N01A	1.502(6)
Ce01	Cl08[1]	2.8213(15)	C00T	C00Z	1.375(8)
Ce01	Cl09	2.9552(13)	C00T	C018	1.384(7)
Ce01	O6	2.487(4)	C00W	C25	1.391(6)
Ce01	O2	2.499(3)	C00X	C017	1.396(6)
Ce02	Cl03	2.8918(13)	C00X	C10	1.392(6)
Ce02	Cl05[2]	2.8795(15)	C00Y	C5	1.386(8)
Ce02	Cl07	2.8432(14)	C00Y	C10	1.388(8)
Ce02	Cl08	2.8657(15)	C014	C13	1.508(8)
Ce02	Cl09	2.8653(14)	C016	C017	1.381(7)
Ce02	Cl0A	2.8528(15)	C016	C5	1.380(8)
Ce02	O3	2.545(4)	C018	C25	1.391(6)
Ce02	O4	2.493(4)	C25	C13	1.511(7)
Cl05	Ce02[1]	2.8796(15)	O3	C3	1.432(7)
Cl08	Ce01[2]	2.8213(15)	C1	O6	1.436(7)
N00K	C13	1.506(6)	C2	O2	1.444(6)
C00N	C00W	1.385(6)	O4	C4	1.429(7)

Table S4. Bond Lengths for *S*-MCC.

Atom	Atom	Length/Å	Atom	Atom	Length/Å
Ce01	Cl03	2.8648(16)	O0D	C0H	1.439(8)
Ce01	Cl04[1]	2.9115(17)	O0E	C0AA	1.449(7)
Ce01	Cl05	2.8454(17)	C00G	C00M	1.505(8)
Ce01	Cl07	2.9507(16)	C00G	C012	1.523(8)
Ce01	Cl08	2.8009(17)	C00G	N014	1.493(8)
Ce01	Cl09	2.8224(16)	N00L	C14	1.504(8)
Ce01	O0B	2.497(4)	C00M	C010	1.387(7)
Ce01	O0D	2.496(5)	C00M	C9	1.395(7)
Ce02	Cl04	2.8811(16)	C00N	C011	1.403(7)
Ce02	Cl05	2.8949(16)	C00N	C8	1.373(9)
Ce02	Cl06	2.8412(16)	C00V	C00Y	1.397(11)
Ce02	Cl07	2.8643(17)	C00V	C9	1.388(9)
Ce02	Cl09[2]	2.8661(17)	C00Y	C015	1.373(10)
Ce02	Cl0A	2.8575(16)	C00Z	C013	1.382(9)
Ce02	O0C	2.491(5)	C00Z	C8	1.391(10)
Ce02	O0E	2.542(5)	C010	C015	1.396(7)
Cl04	Ce01[2]	2.9115(17)	C011	C27	1.382(7)
Cl09	Ce02[1]	2.8661(17)	C013	C27	1.388(7)
O0B	C0F	1.432(8)	C14	C27	1.513(8)
O0C	C00P	1.442(8)	C14	C5	1.511(10)

Table S5. The values of quantum numbers of Ce^{3+}.

	L	S	J	g_J	μ_{cal}/μ_B
R-/*S*-MCC	3	1/2	5/2	6/7	2.535

Table S6. The values of quantum numbers of Ce^{3+}.

	HT		LT	
Sample	*R*-MCC	S-MCC	*R*-MCC	*S*-MCC
θ/T	−41.687±1.917	−63.141±1.200	−0.230±0.091	−0.696±0.150
χ_0/emu·mol^{-1}·Oe^{-1}	$1.225\times10^{-4}\pm2.650\times10^{-5}$	$-1.974\times10^{-4}\pm1.648\times^{-5}$	$1.59\times10^{-3}\pm2.208\times10^{-5}$	$2.02\times10^{-3}\pm2.727\times10^{-5}$
C/emu·K·mol^{-1}·Oe^{-1}	0.845±0.013	1.023±0.009	0.450±0.002	0.416±0.003
R-Square (COD)	0.99996	0.99997	0.99995	0.99986
Adj. R-Square	0.99996	0.99996	0.99995	0.99986
μ_{eff}/μ_B	2.6	2.861	1.897	1.824

Table S7. The parameters of the 2-level equation.

	R-MCC	*S*-MCC
θ/T	−1.403±0.202	−1.875±0.2
$\mu_{eff,0}/\mu_B$	2.045±0.007	1.988±0.007
$\mu_{eff,1}/\mu_B$	3.186±0.005	3.232±0.004
(E_1/k_B)/K	191.117±3.048	161.784±1.648
R-Square (COD)	0.99996	0.99995
Adj. R-Square	0.99995	0.99995
μ_{eff}/μ_B	2.499	2.519

Table S8. The parameters of the 3-level equation.

	R-MCC	*S*-MCC
θ/T	−0.150±0.247	−0.011±0.37
$\mu_{eff,0}/\mu_B$	1.919±0.036	1.778±0.076
$\mu_{eff,1}/\mu_B$	2.272±0.035	2.223±0.043
$\mu_{eff,2}/\mu_B$	3.629±0.028	3.720±0.027
(E_1/k_B)/K	43.202±12.926	27.521±10.476
(E_2/k_B)/K	206.913±11.792	160.714±8.334
R-Square (COD)	0.9998	0.9996
Adj. R-Square	0.9998	0.9996
μ_{eff}/μ_B	2.497	2.512

References

1 Dolomanov OV, Bourhis LJ, Gildea RJ, Howard JAK, Puschmann H. *J Appl Crystallogr*, 2009, 42(2): 339-341

2 Kresse G, Furthmüller J. *Comp Mater Sci*, 1996, 6(1): 15-50

3 Kresse G, Furthmüller J. *Phys Rev B*, 1996, 54(16): 11169-11186

4 Blöchl PE. *Phys Rev B*, 1994, 50(24): 17953-17979

5 Perdew JP, Ruzsinszky A, Csonka GI, Vydrov OA, Scuseria GE, Constantin LA, Zhou X, Burke K. *Phys Rev Lett*, 2008, 100(13): 136406

6 Grimme S, Ehrlich S, Goerigk L. *J Comp Chem*, 2011, 32(7): 1456-1465

7 Wang V, Xu N, Liu J, Tang G, Geng W. *Comp Phys Commun*, 2021, 267: 108033

8 Zhao X, Hu X, Sun M, Luo X, Zhang C, Chen G, Dong X, Zang S-Q. *J Mater Chem C*, 2022, 10(9): 3440-3446

9 Song Z, Yu B, Liu G, Meng L, Dang Y. *J Phys Chem Lett*, 2022, 13(11): 2567-2575

10 Gao J, Zhang W, Wu Z, Zheng Y, Fu D. *J Am Chem Soc*, 2020, 142(10): 4756-4761

11 Li M, Wang YM, Yang LW, Chai ZF, Wang YX, Wang S. *Angew Chem Int Ed*, 2022, 61(37): 202208440

12 Jin KH, Zhang Y, Li KJ, Sun ME, Dong XY, Wang QL, Zang SQ. *Angew Chem Int Ed*, 2022, 61(30): e202205317

13 Wang B, Wang C, Chu Y, Zhang H, Sun M, Wang H, Wang S, Zhao G. *J Alloy Compd*, 2022, 910: 164892

14 Chen J, Zhang S, Pan X, Li R, Ye S, Cheetham AK, Mao L. *Angew Chem Int Ed*, 2022, 61(30): e202205906

15 Yao L, Niu G, Li J, Gao L, Luo X, Xia B, Liu Y, Du P, Li D, Chen C, Zheng Y, Xiao Z, Tang J. *J Phys Chem Lett*, 2020, 11(4): 1255-1260

16 Guan Q, Ye H, Zhu T, Zhang X, You S, Wu J, Zheng Y, Liu X, Luo J. *Adv Opt Mater*, 2023, 11(17): 2202726

17 Song Z, Liu X, Yang C, Wu Q, Guo X, Liu G, Wei Y, Meng L, Dang Y. *Adv Opt Mater*, 2023, 2301272

18 Guan J, Zheng Y, Cheng P, Han W, Han X, Wang P, Xin M, Shi R, Xu J, Bu X-H. *J Am Chem Soc*, 2023, 145(49): 26833-26842

19 Wang Z, Wang X, Chen Z, Liu Y, Xie H, Xue J, Mao L, Yan Y, Lu H. *Angew Chem Int Ed*, 2023, 62(17): e202215206

20 Zhao X, Li N, Peng J, Xu J, Luo P, Dong X, Hu X. *Chem Commun*, 2023, 59(45): 6881-6884

21 Wei Y, Li C, Li Y, Luo Z, Wu X, Liu Y, Zhang L, He X, Wang W, Quan Z. *Angew Chem Int Ed*, 2022, 61(51): e202212685